Changes in the surface irradiance during the total solar eclipse 2020 in Valcheta, Argentina

P F Orte,[1–3]* E Fernández Lajús,[4,5] R P Di Sisto[4,5], E A Wolfram[3,6], A R Lusi[1,2], M G Nicora[1–3], R L D'Elia1[1], F Verstraeten[6], S Papandrea[4], F Carmona[7]

On December 14, 2020, southern South America experienced a total solar eclipse close to the solar noon. The path of totality, about 90 km wide, extended over the continental region from the Chilean west coast to the Argentine east coast, passing through the provinces of Neuquén, Río Negro and the extreme south of Buenos Aires. In order to study the effects on the atmosphere produced by the total eclipse, the Servicio Meteorológico Nacional Argentino (SMN) and Instituto de Investigaciones Científicas y Técnicas para la Defensa (CITEDEF) carried out a surface radiometric monitoring campaign in Valcheta (40.69°S; 66.15°W), Río Negro, Argentina. In this work, we explore the global surface solar irradiance on a horizontal plane (GHI) with the main objective of quantifying the changes in this parameter for cloudy and clear sky atmospheric conditions, combining ground-based measurements and modeling. A solar limb-darkening function was successfully implemented in the calculation of the irradiance at the top of the atmosphere (TOA) during the eclipse. We estimated a significant GHI attenuation of 41 % between the first (C1) and last (C4) contacts of eclipse compared to similar atmospheric conditions without the total eclipse, which represent a daily reduction of 12 %. In terms of irradiation, a reduction of 3360.1 KJ/m^2 was calculated.

* pfacundo.orte@gmail.com

[1] Consejo Nacional de Investigaciones Científicas y Técnicas (CONICET), Buenos Aires, Argentina.

[2] Centro de Investigaciones en Láseres y Aplicaciones, CITEDEF, UNIDEF (MINDEF-CONICET), Villa Martelli, Buenos Aires, Argentina.

[3] CNRS – IRD – CONICET – UBA. Instituto Franco-Argentino para el Estudio del Clima y sus Impactos (IRL 3351 IFAECI), Buenos Aires, Argentina.

[4] Facultad de Ciencias Astronómicas y Geofísicas - Universidad Nacional de La Plata, Paseo del Bosque S/N - 1900 LP, Argentina.

[5] Instituto de Astrofísica de La Plata (IALP), CCT La Plata - CONICET/UNLP, Argentina.

[6] Dirección de redes de Observación, Servicio Meteorológico Nacional, Buenos Aires, Argentina.

[7] Instituto de Hidrología de Llanuras (IHLLA), Universidad Nacional del Centro de la Provincia de BA, Tandil, Argentina.

I Introduction

Solar eclipses are some of the most fascinating natural spectacles that we can experience. Given the frequency of their occurrence throughout the world, and the particularities that each of these phenomena presents, they constitute natural experiments with which various scientific questions can be addressed. In particular, the local effects on the atmosphere in places on Earth where totality, or even partiality, occurs allow us to confront observations

and models in circumstances where there are sudden and short-term changes in solar radiation.

Several experiments have already been carried out in this regard in attempts to understand the response of the atmosphere to these changes. Meteorological parameters, such as temperature, relative humidity, or wind speed, have been measured during solar eclipses, reflecting short-term variations as a consequence of the drastic reduction in the incoming solar radiation (e.g. [1–4]), depending on the eclipse magnitude and the surrounding environmental and local cloudiness conditions [5, 6]. The influence of solar eclipses on cloudiness has also been observed by different authors, which can impact, in turn, the solar irradiance reaching the surface (e.g. [7]).

Likewise, experiments have been carried out to study the changes in the total ozone column. However, some of them have suggested that such variations have not been attributable to eclipse effects, but rather to artifacts introduced in the routine of the measurements or data processing due to the increasing contribution of diffuse radiation against the decreasing direct irradiance caused by the eclipse (e.g. [6, 8–13]).

Observations of surface irradiance at different wavelengths have been carried out with the goal of determining eclipse-induced changes in spectra that reflect a wavelength dependence due to the solar limb darkening (LD), as the eclipse magnitude increases (e.g. [13–15]). Shorter wavelengths have a much stronger effect than longer wavelengths. Wen et al. (2020) [15] also theoretically calculated the impact of cloud optical depth during the eclipse. They showed that the non-eclipse-to-eclipse surface SW flux ratio depends strongly on the obscuration of the solar disk and slightly on the cloud optical depth. These results enabled them to derive the hypothetical SW flux in the absence of eclipse and estimate the impact of the eclipse on the surface broadband SW radiation budget.

On December 14, 2020, a total solar eclipse occurred which was visible throughout the Argentine territory, and whose entire totality path, 90 km wide, crossed the provinces of Neuquén, Río Negro, and the extreme south of Buenos Aires. The town of Valcheta (40.69° S; 66.15° W), Río Negro, Argentina, was chosen to carry out an atmospheric observation campaign. Thus, SMN and CITEDEF set up a monitoring station to study the effects of the total solar eclipse on meteorology, the atmospheric electric field [16], and surface solar irradiance.

The main objective of this work is to estimate the impact of the Total Eclipse of December 14, 2020 on GHI in cloudy and clear sky atmospheric condition with respect to non-eclipse situation combining GHI ground-based measurements and modeling. In determining the effect of the eclipse on the solar irradiance at the surface, it is necessary to first determine the change in solar irradiance at the top of the atmosphere (TOA) along the whole eclipse as a function of time.

The solar irradiance measurements were obtained during the campaign with a broadband pyranometer, while the modeled clear sky irradiance during the eclipse was calculated using a parametric model [17] affected by obscuration of the solar disk of the moon taking into account the limb-darkening effect. Finally, the GHI without eclipse for all-sky conditions was derived following Wen et al. (2020) [15].

Quantifying changes in GHI at the surface during the eclipse contributes to understanding the remarkable impact of the obscuration in reducing solar photovoltaic (PV) generation [18, 19]. Although the timing of solar eclipse events is well known, the meteorological conditions and cloudiness which can affect the generation during the event are much less predictable. In this sense, GHI observations provide essential information to evaluate models or power generation systems.

Section II.i describes the atmospheric monitoring campaign and ground-based observations. Sections II.ii to II.iv describe the methodology implemented to model the GHI during the eclipse and derive the hypothetical non-eclipse GHI at surface. Section III explores the observed and modeled GHI and presents the results. Finally, conclusions are summarized in section IV.
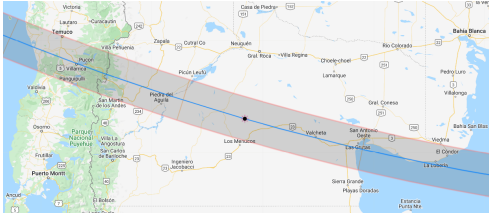
Figure 1: Totality path of the Dec 14th, 2020 solar eclipse. Valcheta is located just about 1 km from the center line and about 100 km from the Greatest eclipse point (black sun)[1].

Figure 2: (left) mobile station installed during the eclipse in Valcheta. (right) Instrumental capability.

II Materials and methodology

i Experiment and Ground-Based observations

The selected site from the totality path of the eclipse was Valcheta (40.69°S; 66.15°W), Río Negro Province (Fig. 1). The eclipse began with the first contact (C1) of the solar and lunar limbs at 11:53 local time (LT), ending at 14:43 LT, when the last contact (C4) between the sun and the moon took place. The duration from the start to the end of this partial phase was 02:50:40.8. The solar limb is understood here by the external edge of its photosphere. The totality elapses between the second contact (C2) at 13:16:23.0 LT and the third contact (C3) at 13:18:32 LT, lasting 2 minutes and 9 seconds. The maximum occurred at 13:17:28 LT when the centers of the sun and the moon reached their minimum distance. In terms of the reduction of radiation, it is important to highlight the closeness between the maximum of the eclipse and the local solar noon ($\sim$ 3 minutes). The magnitude of the eclipse or ratio of the apparent angular diameters of the Moon and Sun for Valcheta was 1.012. All our calculations of these features for the eclipse are summarized in Table 1.

The Global surface solar irradiance at the horizontal plane (GHI) was measured with a broadband pyranometer Kipp&Zonen CMP-21 (285-2800 nm) which was installed on the roof of the mobile monitoring station (Fig. 2). This instrument belongs to the Saver-Net solar radiation network and follows similar measurement protocols to those described in Orte et al., 2021 [20]. The high acquisition frequency of one minute allows for observing the short-term solar irradiance variation due to cloudiness.

In addition, an experimental visible all-sky camera developed by Antuña-Sánchez, J. C. et al. (2015) [21] was reproduced in CITEDEF and installed during the campaign to analyze the cloudiness condition. The camera was configured to acquire images with the same acquisition frequency as the pyranometer (one minute).

For scientific purposes, all datasets are freely available upon request.

ii Modeled GHI for non-eclipse clear-sky condition

The non-eclipse clear-sky GHI for December 14th, 2020 was calculated using the model Global C Iqbal [17, 22]. The date and geographical position that allow for determining the position of the sun throughout the year are included as input parameters in the Global C model. Other inputs are meteorological parameters (temperature, humidity, and pressure at ground level), the total ozone column, and optical characteristics such as ground albedo, Ångström exponent, turbidity coefficient, and the single scattering albedo. Table 2 summarizes the atmospheric and surface parameters used as input in the Global C Model.

The meteorological ground-based parameters

---

[1]http://xjubier.free.fr/en/site_pages/solar_eclipses/TSE_2020_GoogleMapFull.html

Table 1: Main circumstances of the total solar eclipse over Valcheta, Argentina.

Total Solar Eclipse Date: 2020-12-14		
Location		Valcheta / Río Negro
Altitude [masl]		165 m
Geodetic Coord.		Lat: -40.6920 Long: -66.1500
Moon/Sun size ratio		(M2) 1.02529
Maximum Obscuration		100.00 %
Duration of totality		00:02:09.1
Duration of partial eclipse		02:50:40.8
Phase	LT	Alt [°]
Start of partial eclipse (C1)	11:52:56.5	+64.8°
Start of totality (C2)	13:16:23.0	+72.6°
Maximum eclipse (MAX)	13:17:27.6	+72.6°
End of totality (C3)	13:18:32.1	+72.6°
End of partial eclipse (C4)	14:43:37.3	+65.2°

(air temperature (T), relative humidity (H), and pressure (p)) were measured during the campaign using a Campbell meteorological station installed on the roof of the mobile station (Fig. 2). The observations of these parameters at C1 were considered in the GHI calculation for the whole period.

The Total ozone column (TOC) was obtained from the Ozone Monitoring Instrument database (OMI/NASA EOS Aura) retrieved with the DOAS technique (OMDOAO3 L2 overpass data)[2] at 18:55 UTC [23]. The OMI-DOAS TOC presents good agreement compared with ground-based measurements in the region analyzed [24].

On the other hand, the surface albedo was obtained from the CERES SSF1deg product (Edition 4.1)[3]. The hourly gridded instantaneous footprints were average for December 2020 given an albedo value of 0.22. This value was considered as representative of the albedo for December 14th, 2020 due to the very low variability during this month (SD=0.0032). The monthly averaged albedo was also compared with those obtained from land surface downward and upward global radiation obser-

vation (280–2800 nm) carried out by Zheng et al. (2017) [25] for a similar type of soil as Valcheta, obtaining similar values.

The absorption Ångström exponent (α) and the Ångström turbidity coefficient (β) represent the proportion of large or small particles in the aerosol component and the aerosol concentration in the atmosphere, respectively. These parameters were obtained from the monthly climatological values (2005-2021) of the Aeronet observations [4] for December at Trelew city, located 290 km at SSE from Valcheta [26]. While α was obtained directly from the monthly climatology, β was derived for clearing from the following expression:

$$AOD = \beta\lambda^{\alpha} \tag{1}$$

where λ is the wavelength (500 nm) and AOD is the climatological aerosol optical depth.

Finally, a typical value of single scattering albedo (SSA) was introduced [21].

iii Model GHI during the eclipse for clear-sky condition.

The clear-sky GHI during the eclipse was calculated starting from the non-eclipse model de-

---

Table 2: Global C Model inputs parameters.

	Value	Source
T	24 °C	G-B Observation
H	24%	G-B Observation
p	997 hPa	G-B Observation
Albedo	0.22	CERES SSF1deg product
TOC	332.86	OMI
α	0.66	AERONET
β	0.07	AERONET
SSA	0.92	Wong and Chow, 2001.

scribed in the previous section. Then, the attenuation caused by the eclipse is calculated from the sun obscuration between C1 and C4 considering the solar limb-darkening effect following the methodology described in sections II.iii, II.iii, and II.iv.

Calculating eclipses: the evolution of the geometrical configuration

Prediction of eclipses and the calculation of their conditions, geometrical configuration, and duration has obsessed astronomers since earliest times. The calculation and prediction of eclipses involve the precise motions of the Moon, Sun, and Earth, and the location of an observer on the surface of the Earth. This is highly complex and it is necessary to simplify the problem.

This was achieved by the German astronomer Friedrich Wilhelm Bessel, who developed a simplified theory to calculate and predict the local circumstances of solar eclipses by the 1820's. He defined a set of parameters, currently called "Besselian elements", defined in a coordinate system with its origin at the geocenter and oriented to the shadow axis, i.e. z axis, with the x-y plane defining the "fundamental plane". Those elements are in fact geometrical quantities that define the size and orientation of the shadow cone with respect to the surface of the Earth and the fundamental plane for any instant during the eclipse. Therefore, for a specific place on the Earth's surface, the observer's position is transformed to the Besselian coordinate system and the local space and time circumstances are derived.

For this paper, we calculate the geometrical configuration of the eclipse and the evolution over time of specific parameters from the Bessel's method as described in e.g. Seidelmann (1992) [27].

Besselian elements can be calculated using low order polynomial expansions as a function of time. A reference time t_0 in the Terrestrial Dynamical Time (TDT) reference system and the coefficients of these polynomials can be obtained from, e.g. NASA eclipse website[5], based on the Eclipse Predictions by Fred Espenak, NASA's GSFC.

In this way, the Besselian Elements for any instant in a 6 h period, centered on t_0 can be computed. With the calculation of the Besselian elements, and the method described in Seidelmann, (1992) [27], taking into account the correction for flattening of the Earth, we calculate the distance $D(t)$ between the Moon and Sun apparent centers during the whole eclipse as a function of time t. From there, the non-obscured area, or obscuration degree, of the Sun is calculated for the purposes of determining the solar irradiance at the top of the atmosphere for each moment of the eclipse, i.e the light curve.

Limb darkening

The photosphere of the Sun is the layer from which radiation comes, that is, where the optical depth of the different wavelengths (λ) of

---

[5]https://eclipse.gsfc.nasa.gov/SEbeselm/
SEbeselm2001/SE2020Dec14Tbeselm.html

Figure 3: Image of a partial phase of the eclipse taken at 14:04 LT from Valcheta through a 200 mm f/5 Newtonian telescope, using a Canon 70D DSLR camera and a black-polymer. Note the darkening towards the limb of the sun.

the continuum is such that photons can escape through the surface. The optical depth depends on the optical path through the layers of the Sun's atmosphere that photons cross on the way to the surface. Therefore, the critical optical depth is achieved at different depths depending on the observing direction. If we look directly at the center of the Sun, photons originate from inner, and therefore hotter, layers than those we see when looking toward areas near the edge. Then, the sun's disk looks brighter and bluer at its center and darker and redder at its edge. This effect, called "limb darkening" (LD), can be appreciated in Fig. 3.

As a consequence, during a solar eclipse, the variation of the irradiance depends not only on the area covered by the moon but also on the differentiated fluxes that arrive from the center and limb regions, due to LD and its relation to wavelength. For example, in the very early (or late) moments of the eclipse, only part of the weaker limb is covered and the spectrum of the sun seems to be unchanged. But when the eclipse is just before or just after the maximum, the bluer center of the disc is no longer visible, and only a small part of the redder limb region is exposed. At this time the spectrum of the solar irradiation becomes redder. In this way, the monochromatic emission of radiation of the Sun $I_\lambda(r)$ affected by LD depends on the radial distance (r) from the center. The solar irradiance (I_λ^{Tot}) for a certain wavelength emitted by the whole disk can be integrated as follows:

$$I_\lambda^{Tot} = \int_0^{R_\odot} \int_0^{2\pi} I_\lambda^C I_\lambda(r) r d\theta dr \qquad (2)$$

where $R_\odot$ is the radius of the Sun, I_λ^C is the intensity at the center and $I_\lambda(r)$ is the LD coefficient. During the eclipse, the integration limits must be restricted properly considering the eclipse geometry, which is driven by the separation between the centers of the Sun and the Moon, $D(t)$, as explained in the previous section. These considerations and an analytical expression for $I_\lambda(r)$ are given in [14]. We follow in this paper to calculate the TOA solar irradiance. Different wavelengths within the spectral range of the pyranometer were considered here and integrated to obtain the corresponding TOA solar irradiance. Then, the normalized total solar irradiance $I_{norm,tot}$ is defined as the ratio between the irradiance of the not-covered part of the sun and the irradiance of the whole uncovered solar disk, and as such the wavelength range of the pyranometer was retrieved.

To perform the aforementioned calculations of the Bessel method and finally the solar irradiation along the solar eclipse considering LD effects, a numerical code was developed using the GNU/AWK language. It is applicable for any geographic location and was extended to calculate all solar eclipses up to the year 2200, using the polynomial coefficients of the Besselian elements tabulated by Meeus (1989) [28]. A preliminary version of developed application can be run from [6].

Fig. 4 shows the light curve corresponding to normalized solar irradiance I_{norm} with and without considering the LD, corresponding to $\lambda = 280$ nm as an example of the LD effect.

iv Derived GHI for non-eclipse and all-sky condition

Quantifying the decrease in the GHI by the solar eclipse with respect to the non-eclipse
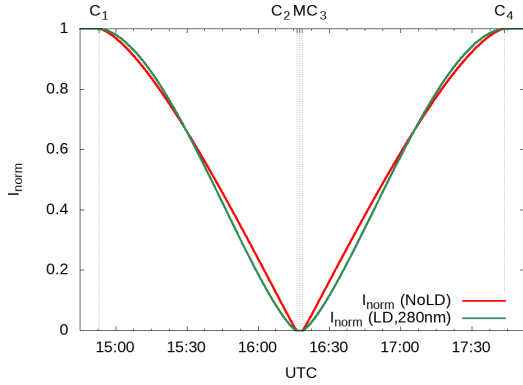
---

[6]http://etacar.fcaglp.unlp.edu.ar/sec/

Figure 4: Eclipse Light curve with no LD (red), with LD (green).

condition is not trivial due to the difficulties in recovering the atmospheric characterization that would have been, without the eclipse. The methodology implemented here consists of combining the ground-based GHI measurement with the clear-sky GHI modeled for both eclipse and non-eclipse conditions. Thus, we derive the GHI that would have reached the surface without the eclipse, in similar atmospheric conditions ($F_{\texttt{non-eclipse}}(t)$), following the method developed by Wen et al. (2020) [15], namely:

$$F_{\texttt{non-eclipse}}(t) \simeq \frac{F_{\texttt{non-eclipse,model}}(t)}{F_{\texttt{eclipse,model}}(t)} F_{\texttt{eclipse}}(t)$$
(3)

wherein, $F_{\texttt{eclipse}}(t)$: Ground-based GHI measurement (section II.i); $F_{\texttt{non-eclipse,model}}(t)$: modeled GHI for clear-sky and non-eclipse conditions (section II.iii); and, $F_{\texttt{eclipse,model}}(t)$: modeled GHI for clear-sky eclipse conditions (section II.ii).

As described, the methodology to obtain $F_{\texttt{non-eclipse,model}}(t)$ developed in section II.iii consists in weighting $F_{\texttt{eclipse,model}}(t)$ by the normalized total solar irradiance integrated for the broadband wavelength range of the pyranometer, ($I_{norm,tot}$). Therefore, under the assumptions described by Wen et al. (2020) [15], $F_{\texttt{non-eclipse}}(t)$ can be approximated directly weighting the measurement $F_{\texttt{eclipse}}(t)$ by $1/I_{norm,tot}$. The modeled GHI for clear sky and for both eclipse and non-eclipse conditions was

useful for evaluating the impact of clouds with respect to the clear sky condition by comparison with this measurement.

Eq. 3 is valid for estimating the GHI for non-eclipse conditions except near the totality. Since the totality covers only 2 minutes and 9 seconds, the derived GHI around 3 minutes of the totality was removed and linearly interpolated. The contribution of this procedure can be considered negligible in terms of the average GHI for the whole eclipse.

III   Results

Fig. 5 depicts the GHI for all-sky non-eclipse situations, considering atmospheric conditions similar to those presented on December 14th for Valcheta, derived from Eq. 3 (red line). The blue line depicts the modeled GHI for clear-sky conditions, including the attenuation due to the eclipse, retrieved applying the methodology developed in Section II.iii which includes the effect of the limb darkening.

The good performance of the implemented model during the eclipse can be observed by comparing it with the observed GHI (black line) during the almost clear-sky period between ~13:55 and ~14:30, where both lines are superimposed. The sky condition was checked from the images of the visible all-sky camera installed. Although there were not total clear-sky conditions, we noted that the direct normal irradiance component and the region around the solar disk was clear in most of this period (Fig. 6 left), with a few cloud fragments passing through FOV in some moments (Fig. 6 right), which explains the very low variation with respect to the measurements.

As was expected, the observation and eclipse-modeled GHI reflect the large reduction between C1 and C4 as a consequence of the solar disk obscuration. The GHI non-eclipse clear-sky derived from the Iqbal model (blue dots) are also included.

Before 10:00 LT the sky was covered by clouds and the direct solar beam was shaded, which explain the large reduction in the observation.
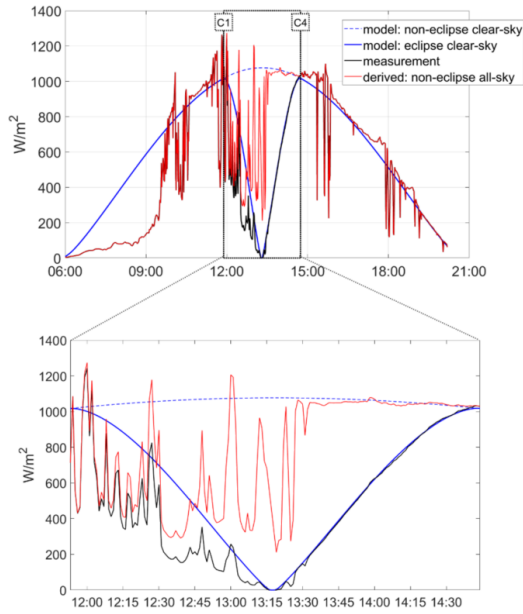
Figure 5: Ground-based GHI measurement (black line), modeled GHI for clear-sky and non-eclipse conditions (dotted line), modeled GHI for clear-sky during the eclipse (blue line) and derive GHI during the eclipse for all-sky conditions (red line). (top) whole day. (bottom) partial and total eclipse period C1-C4.

Figure 6: Images obtained with the visible all-sky camera. (left) almost clear-sky conditions at 14:21 LT. It presents clouds on the periphery of the image and some thin and disperse clouds. (right) cloudiness conditions at 14:07 LT one minute after of a very thin and little cloud fragment passing over the solar disk.

The high variability shown by the observations is attributed to the presence of clouds. From 10:00 LT to C1 (∼11:52 LT), the presence of broken clouds explains the short-term enhancement events (GHI observed (black) above the clear-sky model (blue)). The clouds not shading the solar disk do not attenuate the direct normal irradiance component, while the diffuse component increases by the reflection on the edge of clouds, which enhance the global irradiance above a clear-sky condition [29]. From the sky camera images, we observed that this cloudiness condition was maintained during the period C1 - 13:40 LT, just after the totality, while the TOA solar radiation decreased toward the totality.

At the beginning of the partial eclipse, specifically at minutes 12:00 LT and 12:02 LT, the observation (black line) is above the non-eclipse clear-sky model (blue dots) which reflects that the cloud enhancement dominates against the weak attenuation due to the partial eclipse obscuration.

While the obscuration of the TOA irradiance became more important, the attenuation due to eclipse dominates over the enhancement events. It is observed during two cloud enhancement events at around 12:27 LT and 13:00 LT where the observed GHI (black line) increases above the eclipse clear-sky model (blue) while staying below the non-eclipse clear-sky model (blue dots). The derived GHI (red line) above the clear-sky non-eclipse model (blue dots) indicates that in absence of the eclipse and with similar cloudiness conditions these two events would have enhanced the solar irradiance above that of clear-sky conditions (blue dots) by ∼10% and ∼11%, respectively.

On the other hand, when the derived GHI (red line) is below the eclipse model (blue line), this indicates prevalence of clouds with respect to the eclipse in terms of attenuation. It means that in non-eclipse conditions, the attenuation by clouds would be larger than the attenuation due to obscuration. This is observed mainly between C1 and ∼12:45 LT.

After C4 the impact of broken clouds is observed to lead to abrupt enhancement and attenuation events, similar to the situation just before the partial eclipse.

i Changes in the irradiance budgets

Comparing the derived and the observed GHI, it is possible to estimate the impact of the eclipse in the surface irradiance in Valcheta, Argentina, relative to similar atmospheric conditions but without the eclipse attenuation. We found that the average of the derived GHI (red line) between C1 and C4 was 794.9 W/m^2 while the observation (black line) presents an average value of 469.3 W/m^2. Hence, the reduction in the average surface GHI for Valcheta due to the eclipse was 325.6 W/m2, which represents a 41% reduction respect to non-eclipse conditions between C1 and C4, and a daily reduction of $\sim$12%.

Similarly, if we compare the eclipse clear-sky modeled GHI (blue line) with the observation (black line) we can estimate the reduction due to cloudiness in presence of the eclipse. We estimate that the average GHI reduction due to clouds between C1 and C4 was 118.0 W/m^2. We can note that the TOA GHI reduction due to eclipse (41%) dominates over the reduction due to cloudiness (20%). In terms of irradiation, the impact of the eclipse represents a reduction of 3360.1 KJ/m^2 while the attenuation due to cloudiness is 1198.2 KJ/m^2.

IV Conclusions

A ground-based measurement campaign to observe the changes in the global surface solar irradiance during the total solar eclipse on December 14, 2020, was carried out at Valcheta (40.69°S; 66.15°W), Río Negro, Argentina.

To determine the reduction in the average surface solar irradiance budget, the normalized total solar irradiance $I_{norm,tot}$, defined as the ratio between the total irradiance of the uncovered part of the solar disk and the total irradiance of the whole solar disk for the wavelength range of the pyranometer, was retrieved considering the limb-darkning effect. It was calculated at each minute by a numerical code written in GNU/AWK language. This developed tool can be applied to estimate the normalized total solar irradiance for any geographic location impacted by the total or partial solar

eclipse effect and was extended to calculate all solar eclipses (total, partial or hybrid) up to the year 2200. A preliminary version of this application can be run from [7].

Combining these calculations with the ground-based GHI observation, we estimated a significant GHI attenuation of 41% between C1 and C4 with respect to similar atmospheric conditions without the total Eclipse and a daily reduction of 12%. It represents a total reduction of 3360.1 kJ/m^2 in terms of irradiation.

The reduction in the solar irradiance due to the eclipse has an important impact on solar PV energy generation that has to be considered in the operation of a plant to minimize the consequence of such disruptions for service delivery. The quantification and the observation of changes in the solar irradiance due to the eclipse on 14 December 2020 contributes experience to previous studies to be considered in future scenarios. On the other hand, the numerical code developed is a relevant contribution in a context of PV solar generation growth enabling the prediction of future eclipses and thus forecasting the impact of these phenomena on the irradiance for clear-sky conditions, allowing system operators to analyze in advance the impact on their networks and manage these challenging situations from the point of view of the operation.

---

[7]http://etacar.fcaglp.unlp.edu.ar/sec/
[8]https://www.argentina.gob.ar/noticias/
proyecto-eclipse-solar-2020-valcheta

[1] J Anderson, *Meteorological changes during a solar eclipse*, Weather **54**, 207 (1999).

[2] W Fernandez, V Castro, H Hidalgo, *Air temperature and wind changes in Costa Rica during the total solar eclipse of July 11, 1991*, Earth, Moon Planets **63**, 133 (1993).

[3] W Fernandez, H Hidalgo, G Coronel, et al., *Changes in meteorological variables in Coronel Oviedo, Paraguay, during the total solar eclipse of 3 November 1994*, Earth, Moon Planets **74**, 49 (1996).

[4] K L Aplin, R G Harrison, *Meteorological effects of the eclipse of 11th August 1999 in cloudy and clear conditions*, Proc. R. Soc. Lond. A **459**, 353 (2003).

[5] D Founda, D Melas, S Lykoudis, et al., *The effect of the total solar eclipse of 29 March 2006 on meteorological variables in Greece*, Atmos. Chem. Phys. **7**, 5543 (2007).

[6] E Gerasopoulos, C S Zerefos, I Tsagouri, et al., *The total solar eclipse of March 2006: overview*, Atmospheric Chemistry and Physics **8**, 5205 (2008).

[7] E Hanna, *Meteorological effects of the solar eclipse of 11 August 1999*, Weather **55**, 430 (2000).

[8] Y Kawabata, *Spectrographic observation on the amount of ozone at the total solar eclipse of June 19, 1936*, J. Astron. Geophys. **14**, 1 (1936).

[9] D Stranz, *Ozone measurements during solar eclipse*, Tellus **13**, 276 (1961).

[10] D K Chakrabarty, N C Shah, K V Pandya, *Fluctuation in ozone column over Ahmedabad during the solar eclipse of 24 October 1995*, Geophys. Res. Lett. **24(23)**, 3001 (1997).

[11] C S Zerefos, D S Balis, C Meleti, et al., *Changes in environmental parameters during the solar eclipse of 11 August 1999, over Europe. Effects on surface UV 20 solar irradiance and total ozone*, J. Geophys. Res. **26**, 463 (2000).

[12] M Antón , A Serrano, M L Cancillo, et al., *Solar irradiance and total ozone over El Arenosillo (Spain) during the solar eclipse of 3 October 2005*, J. Atmos. Sol.-Terr. Phy. **72**, 789 (2010).

[13] G Bernhard, and B Petkov, *Measurements of Spectral Irradiance during the Solar Eclipse of 21 August 2017: Reassessment of the Effect of Solar Limb Darkening and of Changes in Total Ozone*, Atmos. Chem. Phys. **19**, 4703 (2019).

[14] P Koepke, J Reuder, J Schween, *Spectral variation of the solar radiation during an eclipse*, Meteorol. Z. **10**, 179 (2001).

[15] G Wen, A Marshak, S -C Tsay, et al., *Changes in the surface broadband shortwave radiation budget during the 2017 eclipse*, Atm. Chem. and Physics, **20 (17)**, 10477 (2020).

[16] Y R Velazquez, M G Nicora, V S Galligani, et al., *The 2020 Patagonian solar eclipse from the point of view of the atmospheric electric field*, Papers in Physics, **14**, 140008 (2022).

[17] M Iqbal, *An Introduction to Solar Radiation*, Academic. Press, Toronto (1983).

[18] H R Giles, H Edward, *The solar eclipse: a natural meteorological experiment*, Phil. Trans. R. Soc. A., **374** (2016).

[19] S K Kurinec, M Kucer, B Schlein, *Monitoring a photovoltaic system during the partial solar eclipse of August 2017*, EPJ Photovolt. (2018).

[20] P F Orte, E Wolfram, E Luccini, et al., *Saver-Net UV-total solar irradiance monitoring network in Argentina*, Revista Meteorológica, Argentina, **47(2)** (2021).

[21] J C Antuña-Sánchez, N Díaz, R Estevan, A M de Frutos, et al., *Cloud camera design using a Raspberry Pi Diseño de una cámara de nubes usando Raspberry Pi*, Experiments in Fluids, **42(3)**, 403 (2015).

[22] L T Wong & W K Chow, *Solar radiation model*, Applied Energy, Elsevier, **69(3)**, 191 (2015).

[23] J P Veefkind, J F de Haan, E J Brinksma, et al., *Total Ozone from the Ozone Monitoring Instrument (OMI) using the DOAS technique*, IEEE Trans. Geosci. Remote Sens., **44**, 1239 (2006).

[24] P F Orte, E Luccini, E Wolfram, et al., *Comparison of OMI-DOAS total ozone column with ground-based measurements in Argentina*, Revista de Teledetección, **57**, 13 (2020).

[25] Z Zheng, Z Wei, Z Wen,et al., *Inclusion of solar elevation angle in land surface albedo parameterization over bare soil surface*, Journal of Advances in Modeling Earth Systems, **9**, 3069 (2017).

[26] B N Holben, et al., *AERONET-A federated instrument network and data archive for aerosol characterization*, Rem. Sens. of Env., **66**, 1 (1998).

[27] S E Urban, P Kenneth Seidelmann, *Explanatory Supplement to the Astronomical Almanac*, University Science Books, California (1992).

[28] J Meeus, *Elements of Solar Eclipses, 1951-2200*, Willmann-Bell, Richmond (1989).

[29] G Pfister, R L Mckenzie, J B Liley, A Thomas, *Cloud coverage based on all-sky imaging and its impact on surface solar irradiance*, J. Appl. Meteorol. **42**, 1421 (2003).